**Electronic Supplementary Information**

# Influence of Halogen Substitutions on Rates of Charge Tunneling across SAM-based Large-area Junctions

Gyu Don Kong,[a] Miso Kim,[a] Hyeon-Jae Jang,[a] Kung-Ching Liao,[b] and Hyo Jae Yoon[a]*

[a]Department of Chemistry, Korea University, Seoul, 136-701, Korea

[b]Department of Chemistry and Chemical Biology, Harvard University, 12 Oxford Street,

Cambridge MA 02138, USA

*Corresponding Author E-mail: hyoon@korea.ac.kr

Experimental Details

*Materials* All reagents were used as supplied unless otherwise specified. All organic solvents were purchased from Sigma-Aldrich or Fisher while water was purified using a Millipore Q-POD water purification system. Bezenethiol (≥99%), *p*-fluorobenzenethiol (98%), *p*-chlorobenzenethiol (97%), *p*-bromobenzenethiol (95%), benzyl mercaptn (99%), *p*-fluorobenzyl mercaptan (96%), *p*-chlorobenzyl mercaptan (98%), *p*-bromobenzyl mercaptan (98%), and high purity eutectic gallium-indium (EGaIn; 99.99%) were obtained from Sigma-Aldrich and used as supplied. *p*-Iodobenzenethiol and *p*-iodobenzyl mercaptan were synthesized following the methods reported in the literature.[1, 2] All thiol derivatives were stored under $N_2$ atmosphere and <4 °C.

*Characterization.* ^{1}H and ^{13}C{^{1}H} NMR spectra were recorded on a Bruker DPX 400 using $CDCl_3$ as a solvent and residual solvents as an internal standard. The contact angle measurements were performed using a contact angle measurement system (Ramé-Hart model 500-F1, Ramé-Hart Instrument Co.) at room temperature (20 – 25 °C) with ~20% relative humidity. The droplet volume for the measurement was ~10 μL. We characterized the SAMs with X-ray photoelectron spectroscopy (XPS; Thermo Scientific K-Alpha photoelectron spectrometer with Monochromatic Al K-α X-ray radiation (1.49 kV at base pressure ~$10^{-9}$ Torr)).

*Experimental Details for Preparation of SAMs.* We prepared SAMs following the procedure reported previously.[3] Toluene (anhydrous, 99.8%; Sigma-Aldrich) solution (3 mM) of each of HS($p$-$C_6H_4X$) molecules (X=F, Cl, Br, and I) was added to an amber-colored vial. The solution was sealed and degassed by bubbling $N_2$ through the solution for *ca*. 1 min. Ag$^{TS}$ was washed

with pure toluene, and placed to the solution of the thiol with the exposed metal face up. The vial was then filled with $N_2$. After 3 h incubation at room temperature, the $Ag^{TS}$ film with the SAM on it was removed from solution and rinsed by repeatedly dipping the chip into clean toluene (3 × 1 mL). The solvent on the SAM was then evaporated by blowing gently a stream of nitrogen over chip.

*Experimental Details for Electrical Measurements.*

*Tip formation.* EGaIn conical tip was formed following the method reported in the literature.[4-6] To generate a conical tip of EGaIn for use as a top contact, a 10 μL gas-tight syringe was filled with EGaIn (≥99.99%, Sigma-Aldrich). A drop of EGaIn was then pushed to the tip of the syringe needle, the hanging drop was brought into contact with a surface on which the EGaIn would stick (e.g., an oxidized Ag surface), and the needle gently pulled away from the drop using a micromanipulator. Upon breaking from the bulk EGaIn on the surface, a fine conical shaped tip was obtained. Tip was newly formed every three junctions. In cases that visible whiskers formed during tip fabrication, we discarded the tip and formed a new tip; therefore, our junction measurements were carried out using "selected" conical tips that did not contain observable filament during tip formation.

*Junction Formation and Measurements.* Junction formation and measurements were done following the method reported in the literature.[4-6] A SAM on $Ag^{TS}$ was gently brought into contact first with a gold metal electrode. Then using a micromanipulator, conical EGaIn tip was gently brought into contact with its own reflection on the Ag surface, at which point a conformal contact has been established between the SAM and the EGaIn tip. The contact area was derived

from measuring the diameter of the contact area at high magnification. Assuming a circular contact, the area was derived from the measured diameter from which the current densities were calculated. The contact and presence of a SAM was confirmed by running a single *J-V* scan after which 20 more scans were run if there was indication of contact and tunneling. The total number of working junctions versus those that shorted was used to calculate the yield (%) of working junctions. Junction measurements were done with 3-4 samples by multiple users.

Minor Discussions

*Structure-Property Relations at the Top-interface in EGaIn Tunneling Junctions.* The role of the top interface (the interface between the terminus (denoted as "X" in this work) of SAM and the $Ga_2O_3$ surface of EGaIn electrode) in charge transport across EGaIn-based junctions is not known exactly. In an effort to resolve this issue, Whitesides and coworkers[3, 4, 7] have previously introduced many functional groups into the X region and used to examine effects of compositional changes at the $X//Ga_2O_3$ interface on the rates of charge tunneling across $Ag^{TS}/S(CH_2)_nM(CH_2)_mX//Ga_2O_3/EGaIn$ junctions (where M is the middle moiety of the SAM, either $-CH_2CH_2-$ or $-CONH-$).[3, 8] Rather surprisingly, *J*(*V*) through these junctions was not significantly affected by structural variations at the $X//Ga_2O_3$ top interface that involve simple aromatic/aliphatic groups,[3] uncharged polar groups having a wide range of dipole moments $(0.5 < \mu < 4.5)$,[4] and Lewis acidic/basic groups capable of forming ionic and/or hydrogen bonds with the $Ga_2O_3$ surface.[7]

*Characterization of HS(CH$_2$)$_n$(p-C$_6$H$_4$X) Compounds.* All thiols were characterized using ^{1}H NMR spectroscopy (see Figures S7 - S15 for NMR spectra) prior to use for preparation of SAMs.

^{1}H NMR spectra for benzenethiol, *p*-fluoro- and *p*-chloro-benzenethiols, benzyl mercaptan, and

*p*-fluoro-, *p*-chloro-, *p*-bromo- and *p*-iodo-benzyl mercaptans did not show peaks related to

oxidized byproducts. Although bromine- and iodine-terminated benzenethiols (HS(*p*-C$_6$H$_4$Br)

and HS(*p*-C$_6$H$_4$I)) were purified through silica-gel column chromatography (one spot in TLC

analysis was confirmed during purification), ^{1}H NMR spectra for bromine- and iodine-

terminated benzenethiols (HS(*p*-C$_6$H$_4$Br) and HS(*p*-C$_6$H$_4$I)) showed minor peaks in the aromatic

region (7 - 8 ppm) that are indicative of formation of disulfide (not other oxidized products such

as sulfonate, sulfone, and sulfoxide) in CDCl$_3$ during preparation of NMR sample (or during

measurements). This small amount of disulfide did not provide defects or structurally different

thiolates in SAMs that are detectable by XPS: characterization of Ag$^{TS}$/S(*p*-C$_6$H$_4$X) SAMs using

XPS (see below) confirmed that all the S(*p*-C$_6$H$_4$X) SAMs we studied contain one type of sulfur

corresponding to thiolate.

*XPS Measurements of Ag$^{TS}$/S(p-C$_6$H$_4$X) Samples.* XPS analysis was performed for surveying

composition of SAMs: in particular, using XPS we wished to determine whether SAMs contain

oxidized forms of thiolates such as sulfonate, sulfone, sulfoxide, or disulfide (due to easily

oxidizable characteristic of arylthiols in the presence of oxygen gas). XPS spectra (Figure S1) for

all of Ag$^{TS}$/S(*p*-C$_6$H$_4$X) samples showed a single type of sulfur, i.e., thiolate (2p$_{3/2}$ and 2p$_{1/2}$ in

~162 eV and ~163 eV),[9] indicating that there were no detectable signals for oxidized byproducts

(sulfonate, sulfone, disulfide, or sulfide).

    The SAM of benzenethiolate showed the presence of other S2p peaks (as minor peaks)

appearing in ~160.5 eV and ~161 eV, which are indicative of the unbound (physisorbed) thiol;[9]

we prepared multiple samples of benzenethiolate SAM and thoroughly rinsed them with pure

toluene several times but repeatedly observed the presence of XPS peaks of unbound thiol. The presence of small amount of unbound (i.e., mobile) thiols does not influence junction measurements: if the unbound thiols affect junction measurements, we would observe decrease in $J(V)$ as compared to the molecular junction comprising a SAM of phenylene of similar thickness. Indeed, the mean value ($\log|J(-0.5V)|_{mean} = 2.5 \pm 0.3$) of current density for the benzenethiolate SAM was compatible with that for the benzenecarboxylate SAM ($\log|J(-0.5V)| = 1.5 \pm 0.2$) measured using the same EGaIn conical electrode.[5] (It has been demonstrated in ref. 5 that replacing a thiolate anchoring group with a carboxylate group does not sifniciantly influence $J(V)$).

All of SAMs that we tested showed small oxygen peaks. We attribute these oxygen peaks to water molecules physisorbed on the surface of the SAM, not to the oxidized byproducts. (Note that none of SAMs studied in this work showed XPS peaks of sulfur atom(s) related to the oxidized byproducts.)

For the iodine-terminated SAM ($S(p\text{-}C_6H_4I)$) a set of small shoulder peaks (~619 eV and ~631 eV) was observed in the deconvoluted high resolution XPS spectrum for iodine atom (Figure S1). The ratio of integrated areas of these small peaks to the major peaks at ~621 eV and ~631 eV was ~0.18. The small peaks are attributed to the lowest dissociation energy of C-I bond among other C-X bonds, leading to thermal scission of C-I bond upon irradiation of X-ray beam or oxidative addition by silver surface that give semi-ionic C-I or Ag-I bonds.[10-12] These peaks are very small as compared to the other iodine peaks, and thus our junction measurements for $Ag^{TS}/S(p\text{-}C_6H_4X)//Ga_2O_3/EGaIn$ junctions are dominated by majority of $SC_6H_4I$ molecules.

*Contact Angle Measurements of Ag$^{TS}$/S(p-C$_6$H$_4$X) Samples.* Static contact angles averaged from nine measurements for wetting by water (10 µL) ranged from 84$^o$ to 91$^o$ (Table S2 and Figure S16). The measured values of wettability for Ag$^{TS}$/S(p-C$_6$H$_4$X) were similar to the reported values for *n*-alkanethiolates of similar length (~85$^o$ for *n*-pentanethiolate) on silver.[13]

*Low Yields of Working Junctions at Applied Bias |V| > 0.5V.* We found significantly decreased yields of working junctions when applied bias is > |0.5V|. For EGaIn-based tunneling junctions, shorter SAMs (e.g., shorter than *n*-octadecanethiolates) usually show significantly decreased yields of working junctions due to the disorder of SAM structure, and an increased electric field (larger than ~3 MV/m,[14] a dielectric strength for air). Electrical short has nothing to do with the electronic structure (HOMO or LUMO) of molecules within junctions. They are related to the property of protective layer (Ga$_2$O$_3$ layer) in the EGaIn top electrode, and degree of structural disorder in SAM.[6]

*Lower Yields of Working Junctions of S(CH$_2$)$_n$(p-C$_6$H$_4$X) SAMs than n-Alkane-based SAMs.* The yields of working junctions for S(CH$_2$)$_n$(p-C$_6$H$_4$X) SAMs ranged from 67 to 71%. These were slightly lower than those (80 – 100%) for SAMs of long *n*-alkanes (SC$_8$ to SC$_{16}$). Plausible explanations for the lower yields of working junctions in SC$_6$H$_4$X SAMs are that i) thin S(CH$_2$)$_n$C$_6$H$_4$X molecules are exposed to higher electric field than thick alkanes at ±0.5V, and/or ii) highly packed *n*-alkanethiolate SAMs show higher yields of working junctions than S(CH$_2$)$_n$(p-C$_6$H$_4$X) SAMs.

*Effects of Halogen Substitutions on the Shape of Tunneling Barrier.* Polarizability is a physical-organic parameter that represents how electron clouds of molecules respond to an external electric field: i.e., how well an electron cloud is distorted in response to an electric field applied. Incorporating easily polarizable molecules into molecular junctions, in principal, leads to instantaneous dipole moment in the presence of high electric field, Thus the halogen-terminated benzenethiolates we studied in this work may form such a dipole moment under a high electric field (~1GV/m for ~1 nm of SAM at 0.5V) and thus change the shape of tunneling barrier of the junction.

Halogens have a different principal quantum number ($n$) but the same electron configuration in the outmost orbital shell (i.e., $n\mathrm{p}^5$; $n = 2 - 5$). The similarity in the electron configuration and the discrepancy in the principal quantum number offer the opportunity to examine the effect of ionization energy that is associated, intuitively, with the energy of highest occupied molecular orbital HOMO, on the rate of charge tunneling.

**Table S1.** Literature Values of Polarizability, Molecular Dipole, Length and HOMO/LUMO

Levels for Monohalogenated Benzenes (as Model Structures for halogenated benzenes).

| X | Polarizability $(\alpha, 10^{-24} \text{ cm}^3)$[a] | Dipole moment $(\mu, \text{D})$[b] | Bond dissociation energy (kcal/mol)[c] | HOMO (eV)[a] | LUMO (eV)[a] |
|---|---|---|---|---|---|
| H | 10.3 | 0.00 | 113 | -9.75 | -0.40 |
| F | 10.3 | 1.60 | 126[b] | -9.80 | -0.027 |
| Cl | 12.3 | 1.69 | 96[b] | -9.39 | -0.063 |
| Br | 13.6 | 1.70 | 80[b] | -9.81 | -0.051 |
| I | 15.5 | 1.70 | 65[b] | -9.04 | -0.43 |

[a]Values were obtained from the literature.[15]
[b]CRC Handbook of Chemistry and Physics (85th Edition, CRC Press)
[c]Handbook of Bond Dissociation Energies in Organic Compounds.

**Table S2.** Summary of Data of Contact Angle Measurements.

| X in S($p$-C$_6$H$_4$X) | $\theta^a$ |
| --- | --- |
| H | $87.1 \pm 3.4$ |
| F | $87.3 \pm 2.5$ |
| Cl | $89.5 \pm 2.9$ |
| Br | $91.1 \pm 2.7$ |
| I | $84.1 \pm 4.9$ |

[a]Value averaged from nine measurements; error range is based on σ (standard deviation).

**Figure S1.** XPS spectra for SAMs of S($p$-C$_6$H$_4$X) on template-striped silver substrate (Ag$^{TS}$).
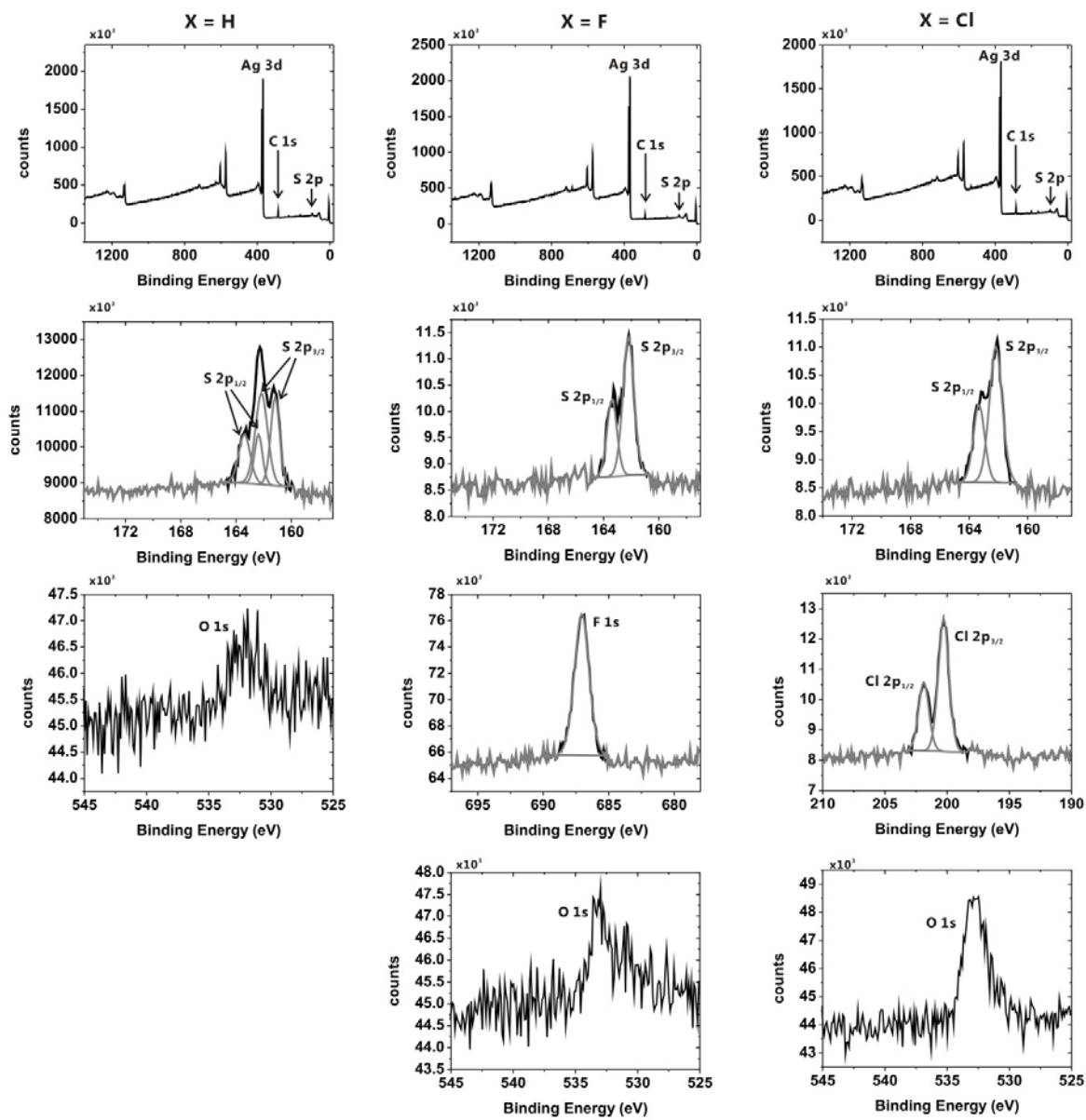
**Figure S1** (continued)
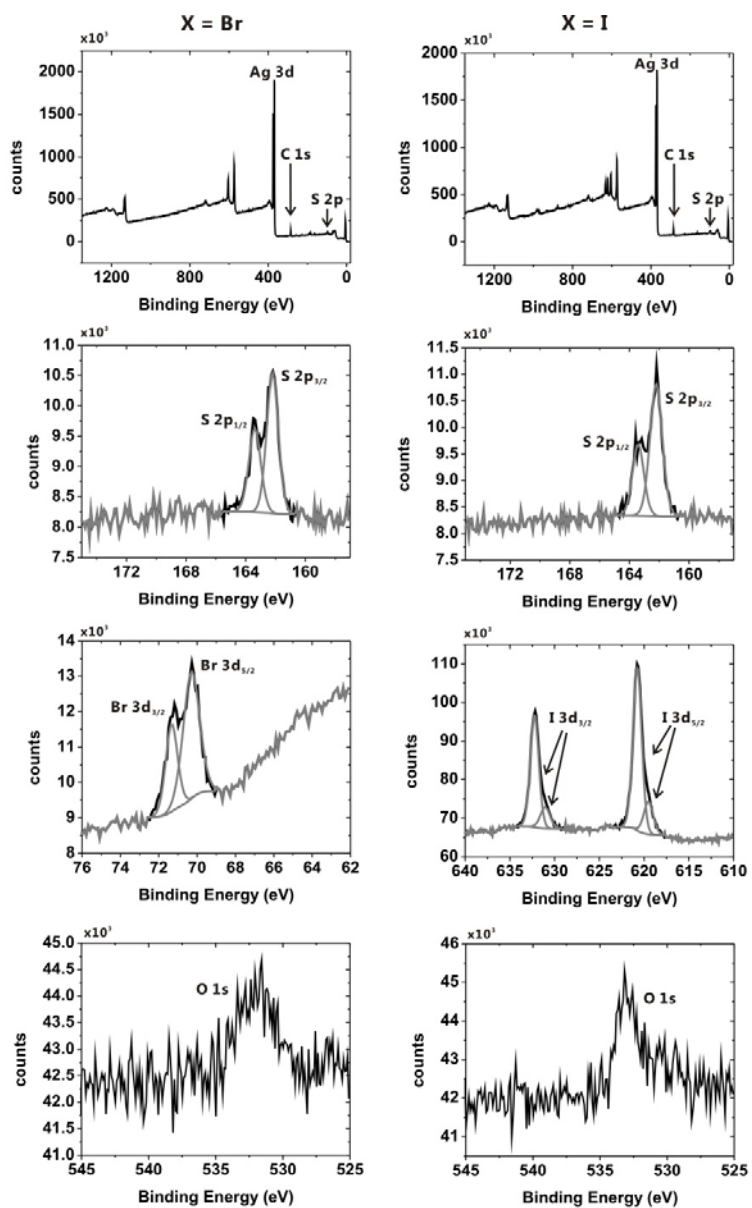
**Figure S2.** Histograms of log|*J*| at ±0.5 V for SAMs composed of benzenethiolates (S(*p*-C₆H₄X)) terminated with a hydrogen (a) or halogen atoms (b–e). (Data of shorts were excluded for clarity).
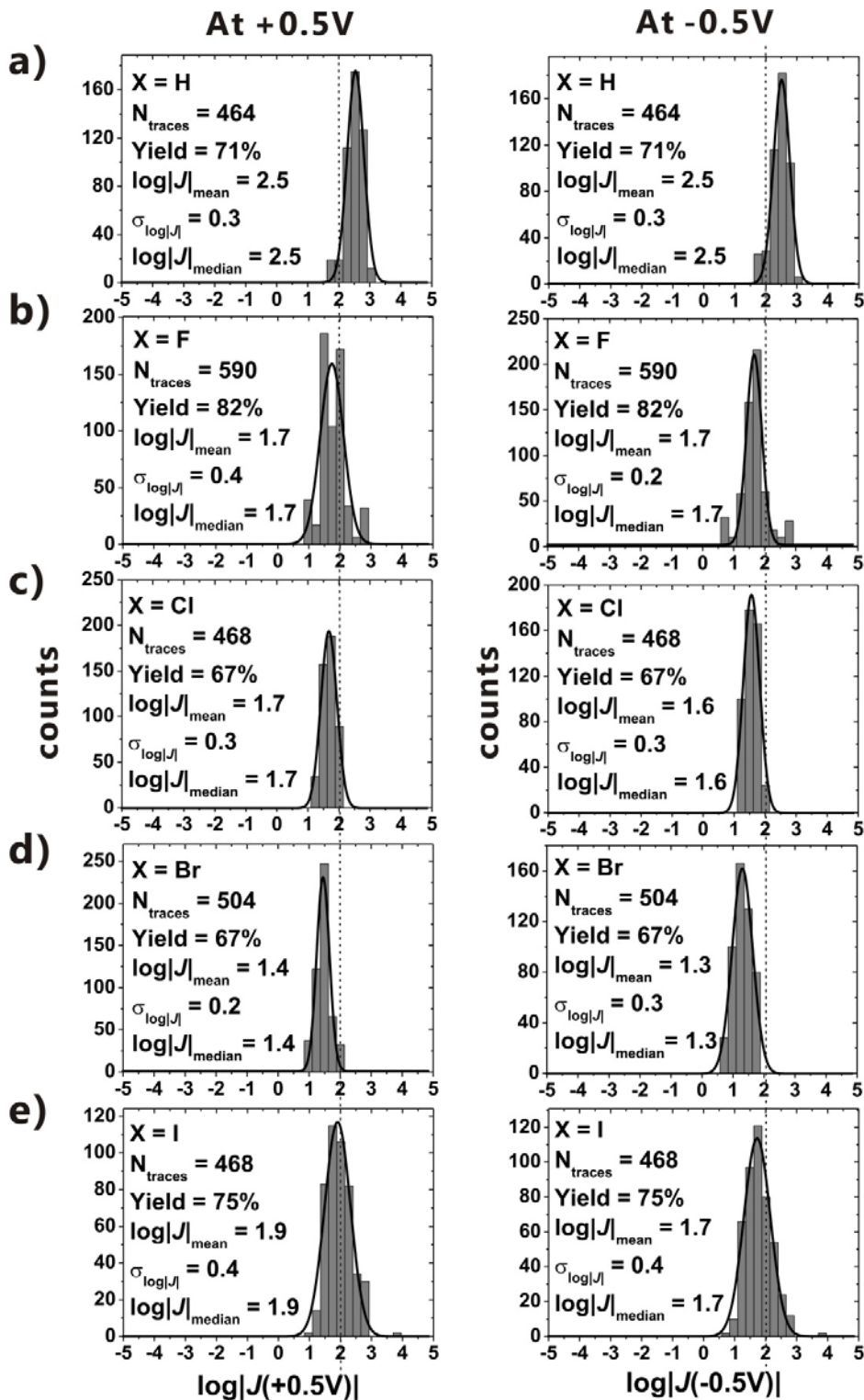
**Figure S3.** Histograms of log|$J$| at ±0.5 V for SAMs composed of benzyl thiolates (SCH$_2$($p$-C$_6$H$_4$X) )terminated with a hydrogen (a) or halogen atoms (b–e). (Data of shorts were excluded for clarity).
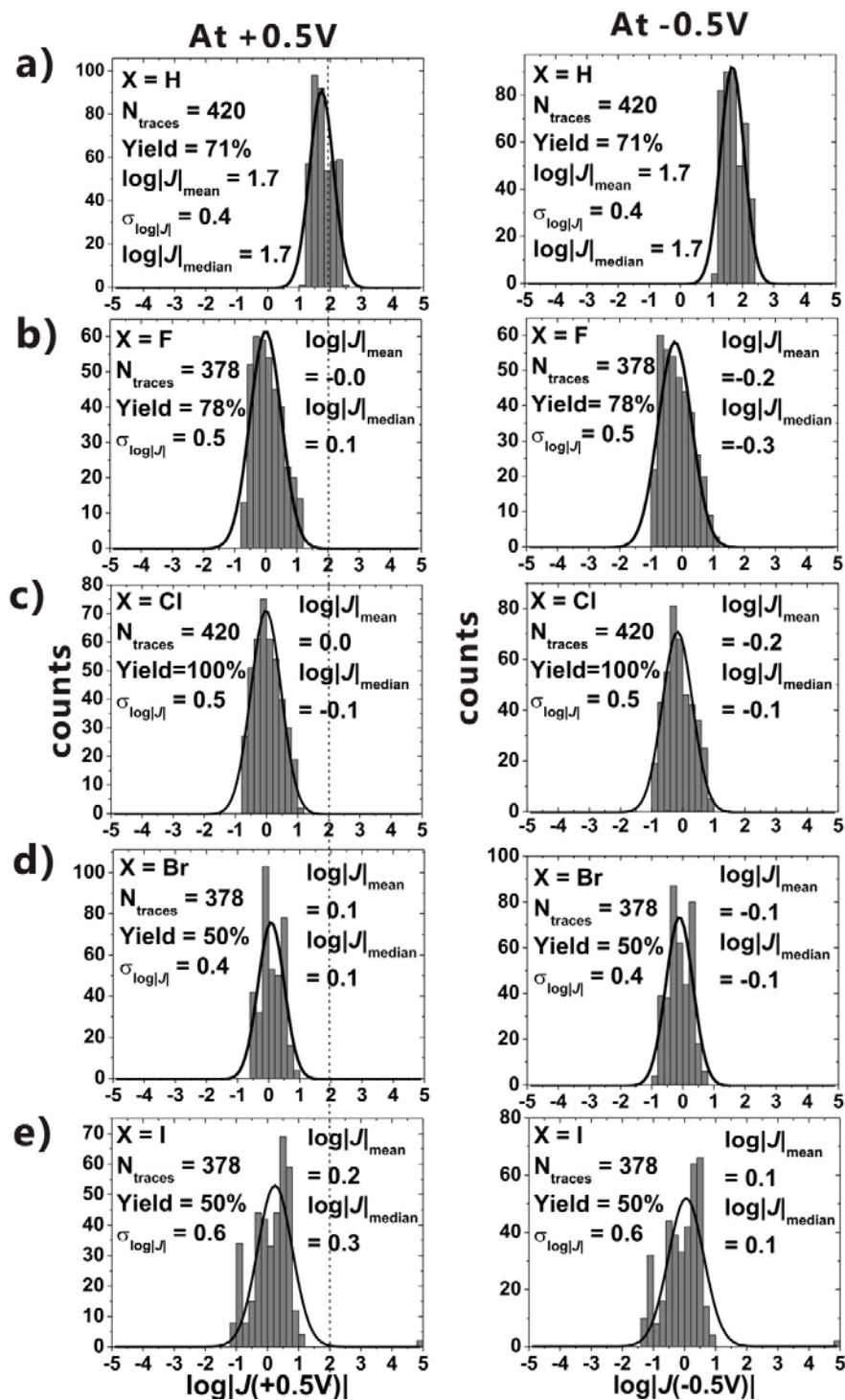
**Figure S4.** Histograms of log-rectification ratio ($\log|r|$, $r = |J(+0.5\ \text{V})|/|J(-0.5\ \text{V})|$) of $\text{Ag}^{\text{TS}}/\text{S}(\text{CH}_2)_n(p\text{-}C_6H_4X)//\text{Ga}_2O_3/\text{EGaIn}$ junctions. a) X=H and b-e) X=halogen.
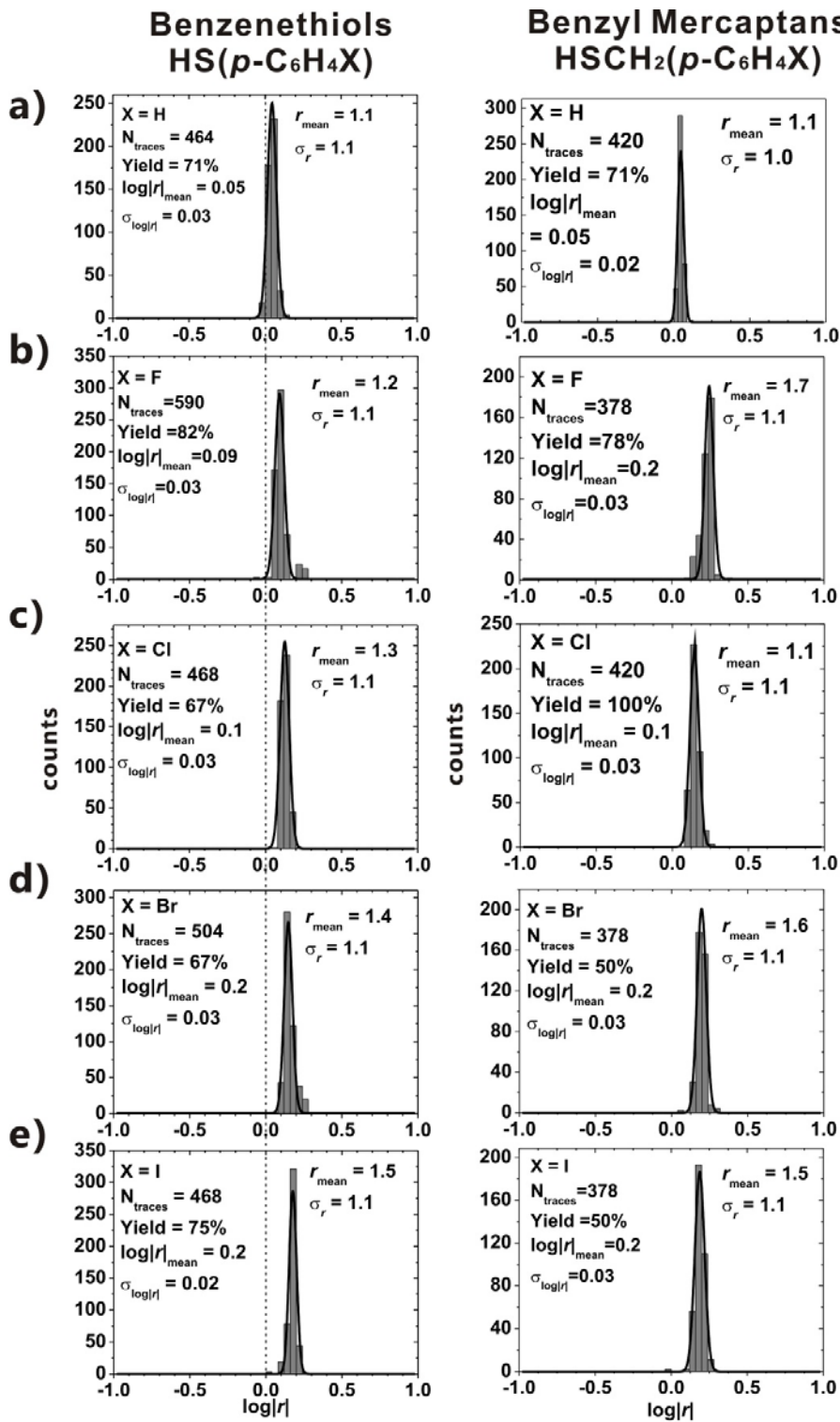
**Figure S5.** Shorting junction under higher bias than ±0.5V. The numbers and arrows indicate the sequence of voltage sweep.
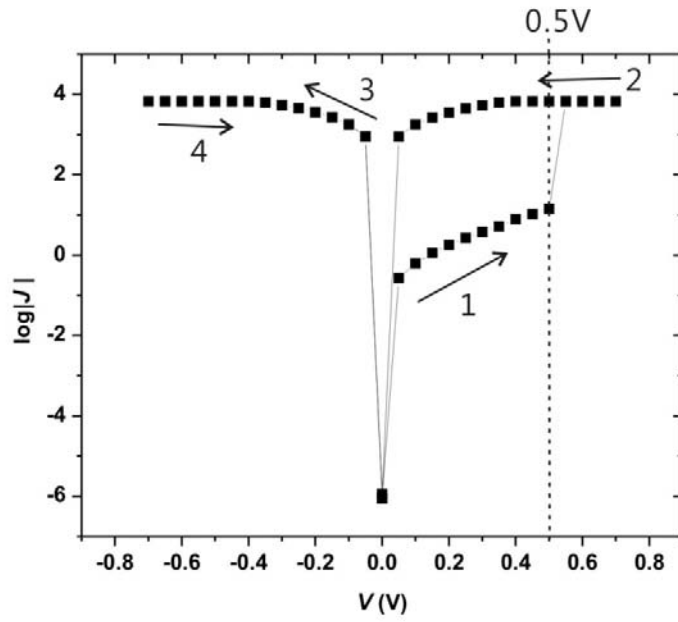
**Figure S6**. Plots of values of $\log|J(+0.5V)|_{mean} \pm \sigma_{log}$ for $Ag^{TS}/S(CH_2)_n(p\text{-}C_6H_4X)//Ga_2O_3/EGaIn$ (n=0, 1) junctions as a function of (a) polarizability ($\alpha$, $10^{-24}$ cm$^3$) at 0V; (b) HOMO (eV); (c) LUMO (eV); and (d) dipole moment ($\mu$, D). Values for benzene and monohalogenated benzenes ($C_6H_6$ and $C_6H_5X$ as a model structure) were obtained from the literature[15] and CRC Handbook of Chemistry and Physics (85th Edition).
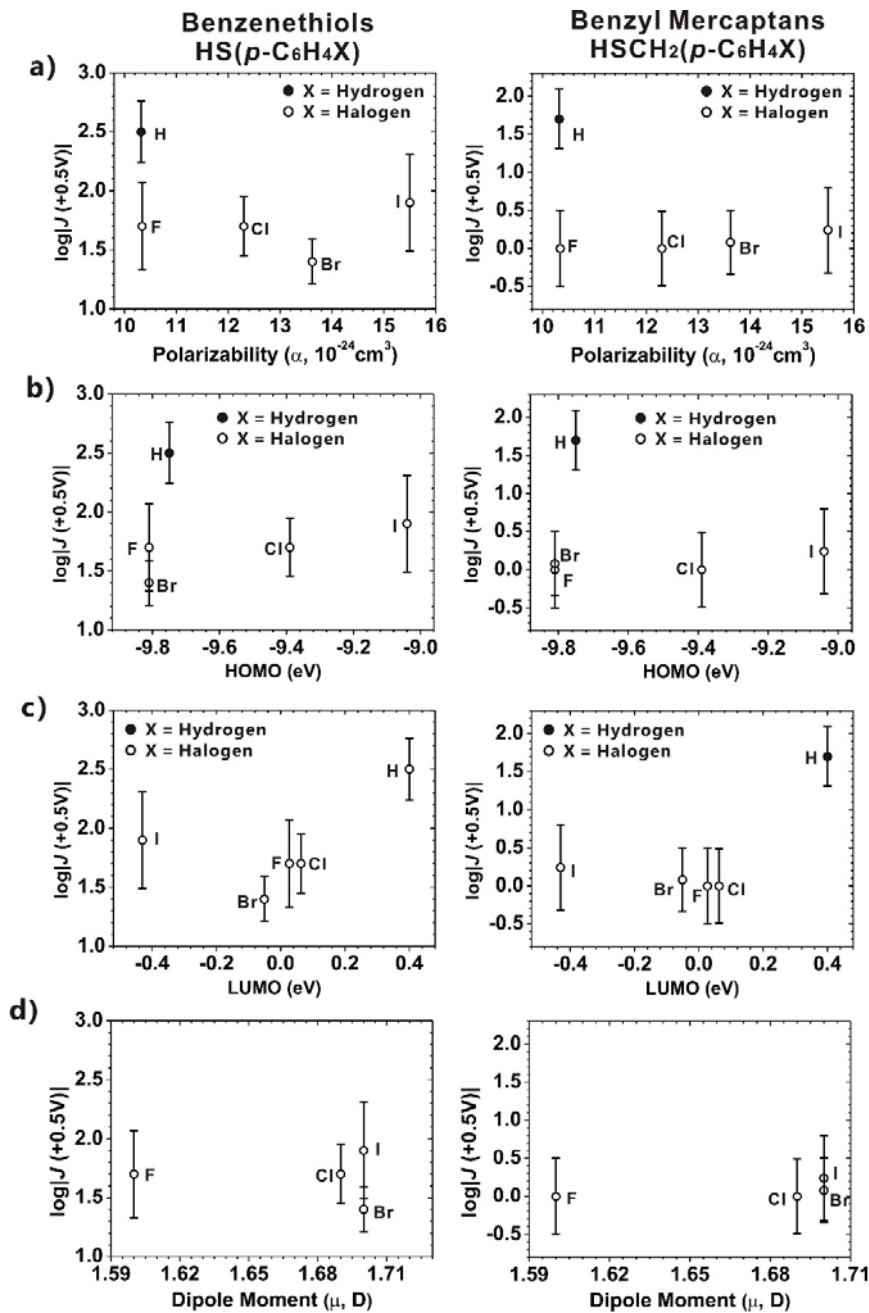
**Figure S7.** $^1$H NMR spectrum for *p*-iodobenzenethiol in CDCl$_3$
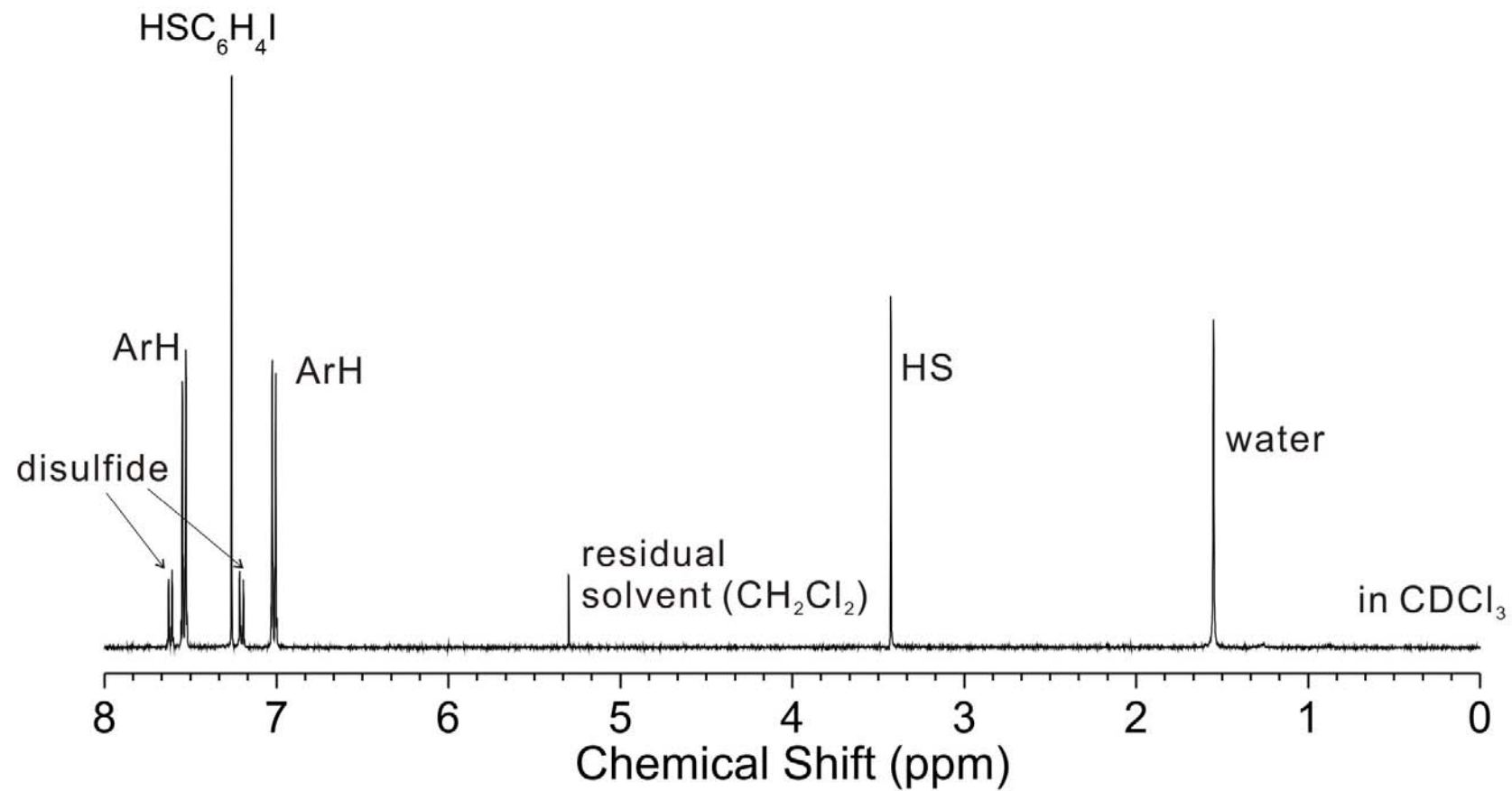
**Figure S8.** $^1$H NMR spectrum for *p*-bromobenzenethiol in CDCl$_3$
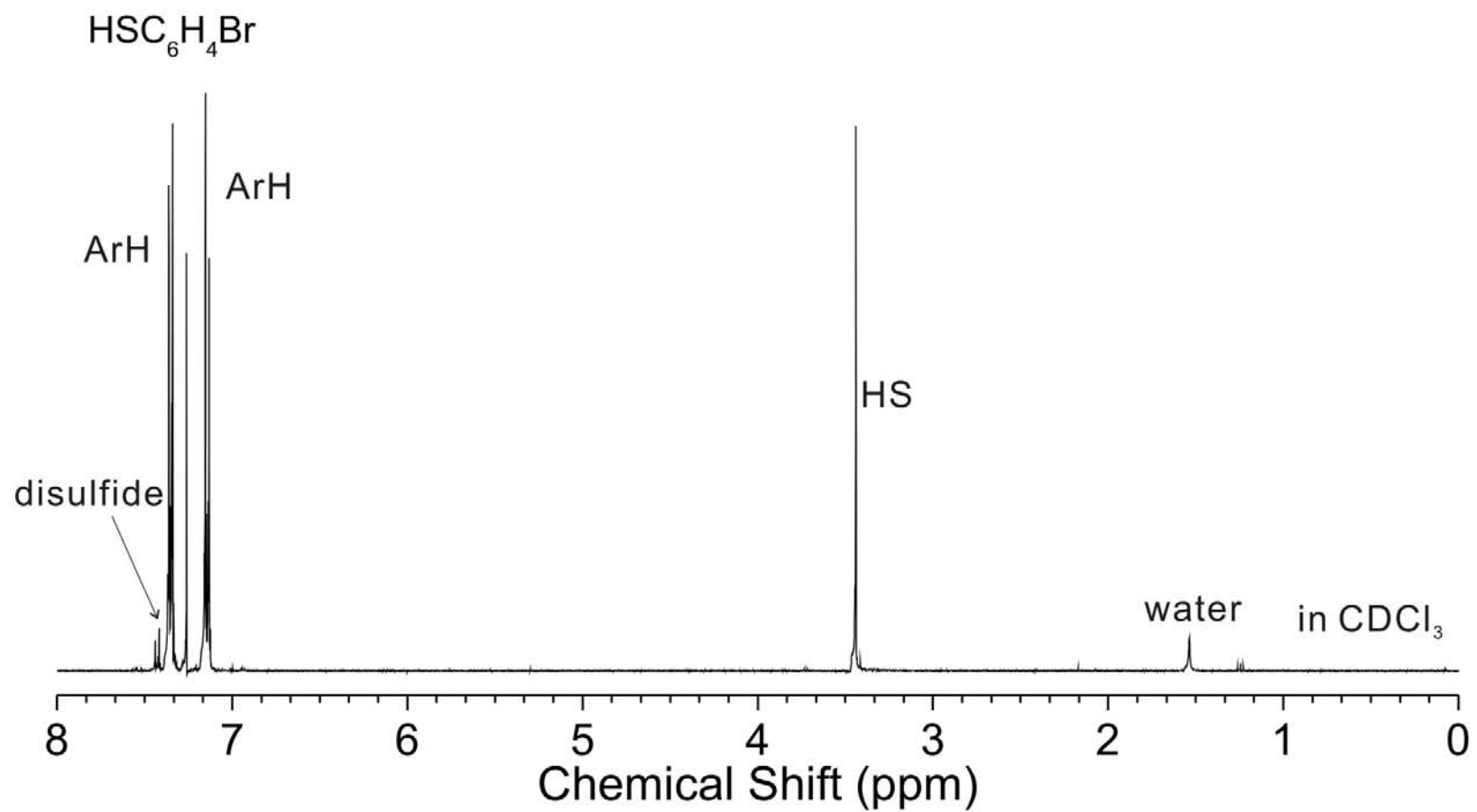
**Figure S9.** $^{1}$H NMR spectrum for *p*-chlorobenzenethiol in CDCl$_3$
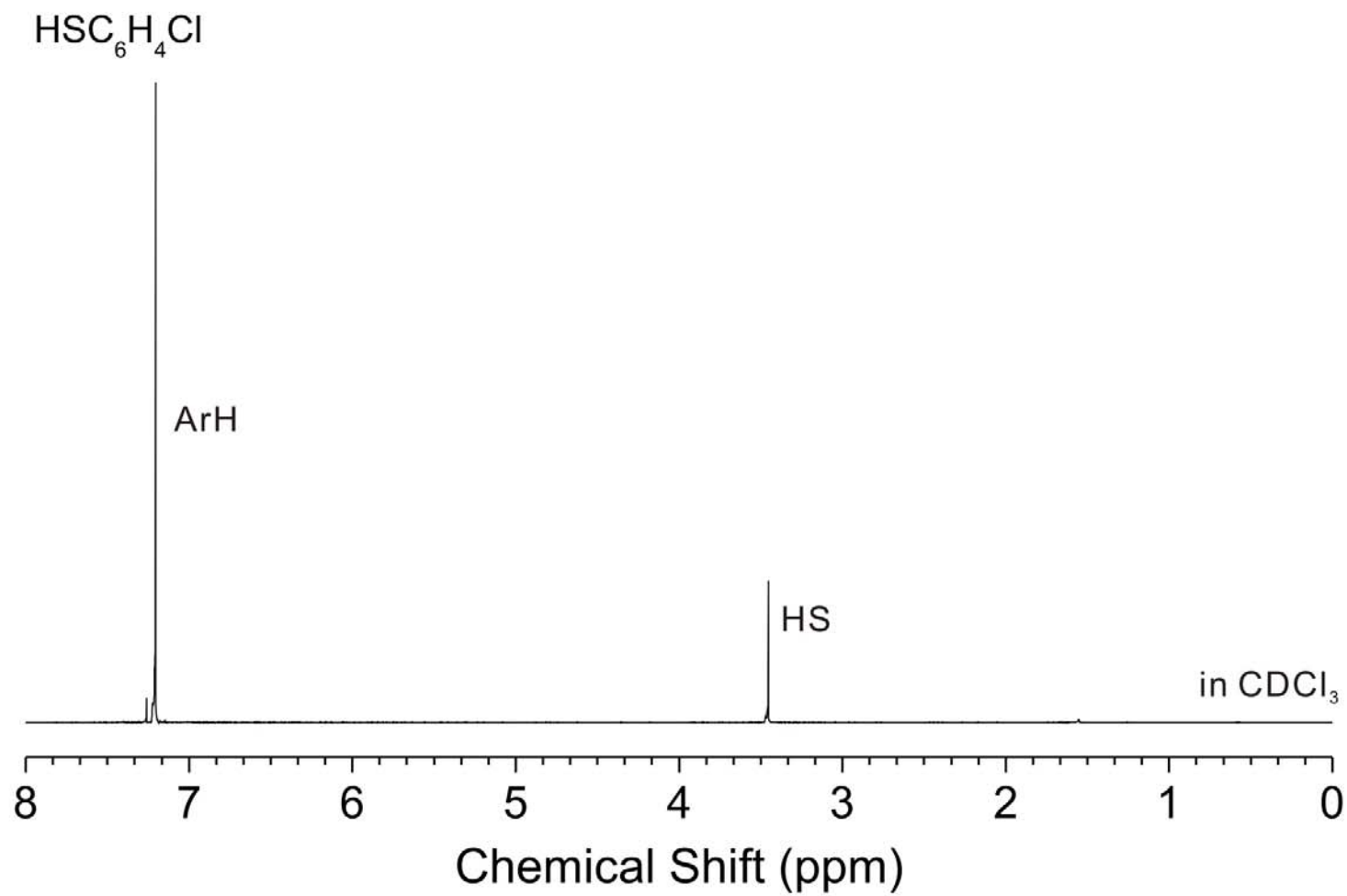
**Figure S10.** $^1$H NMR spectrum for *p*-fluorobenzenethiol in CDCl$_3$
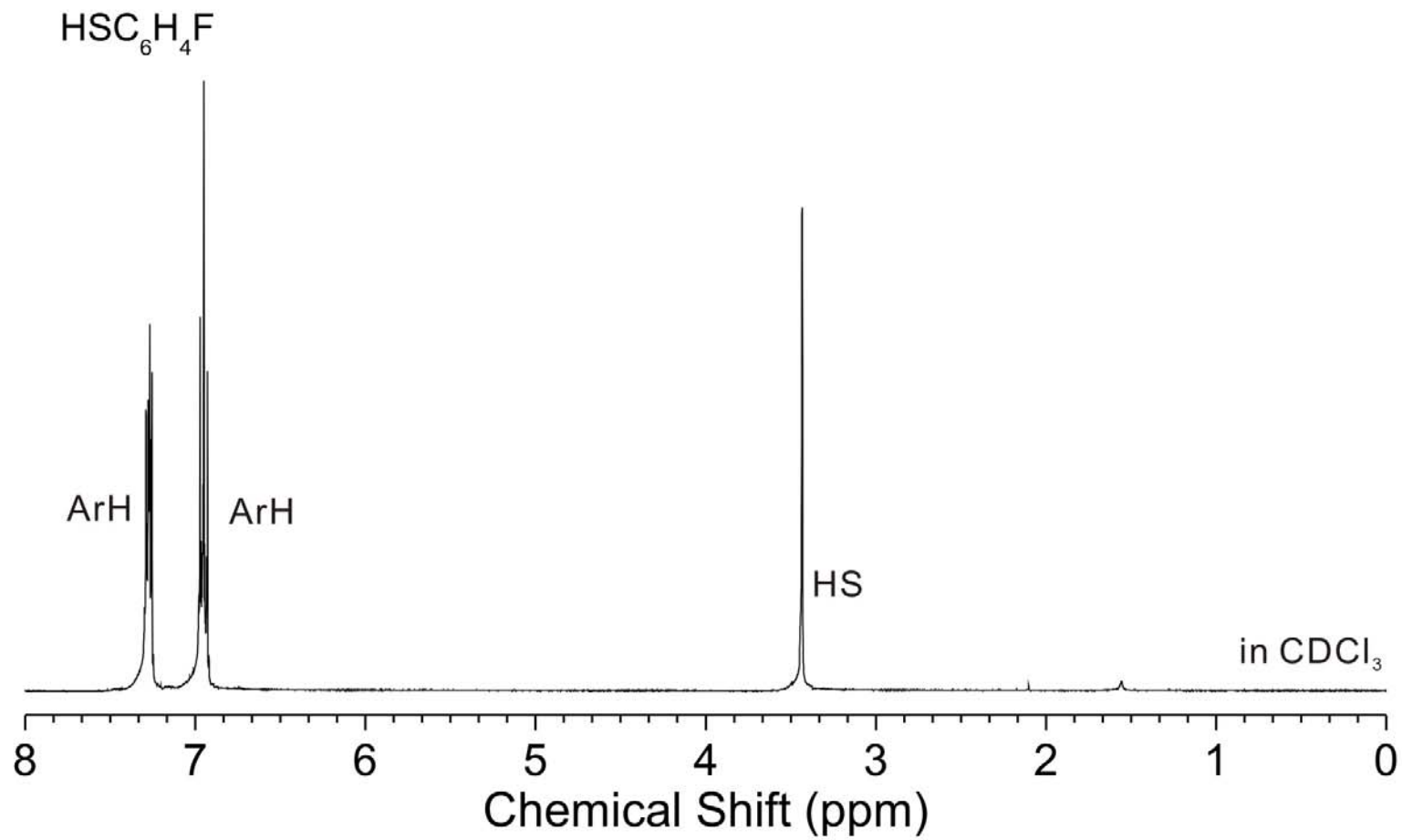
**Figure S11.** $^1$H NMR spectrum for benzenethiol in $CDCl_3$
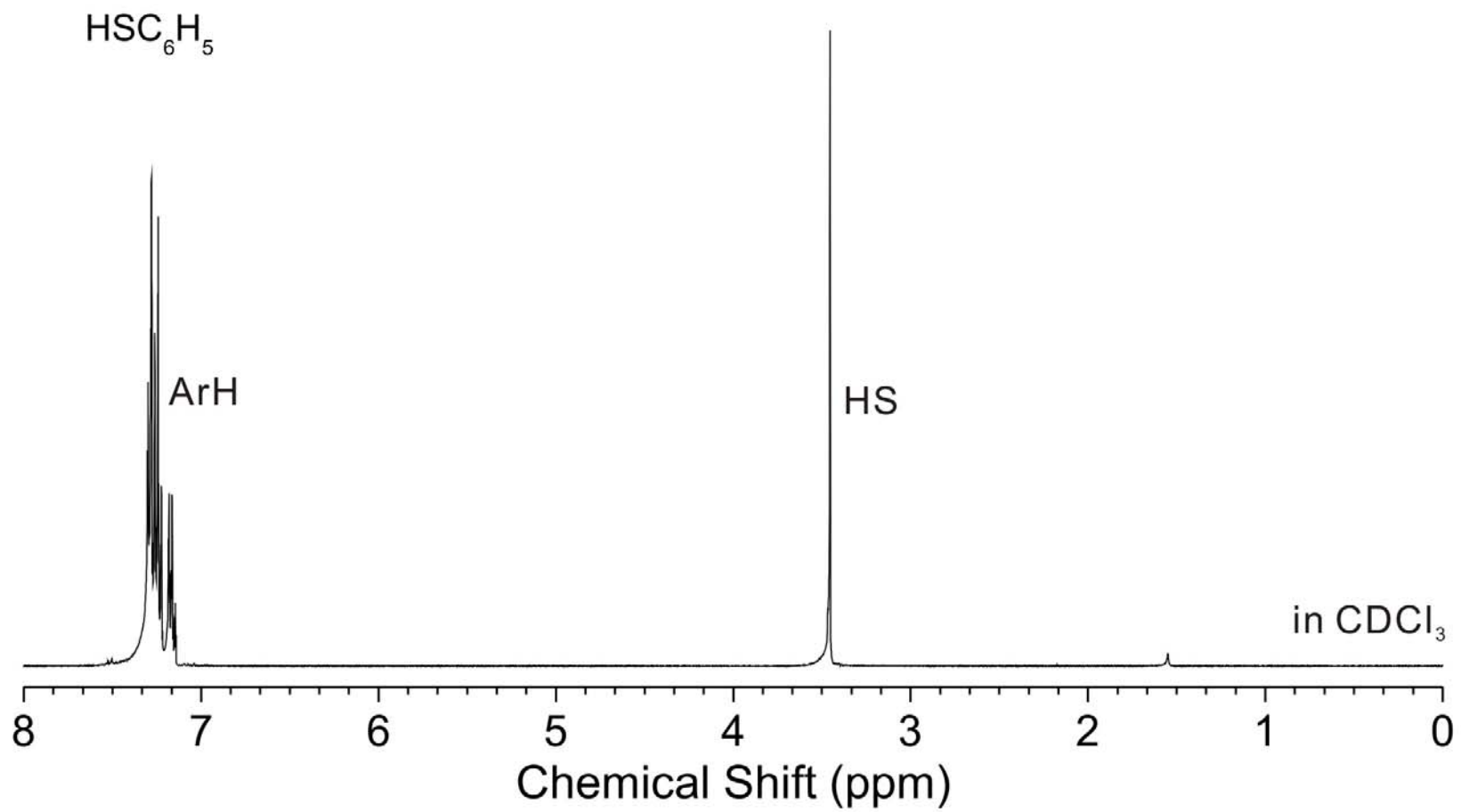
**Figure S12.** $^1$H NMR spectrum for *p*-fluorobenzyl mercaptan in CDCl$_3$
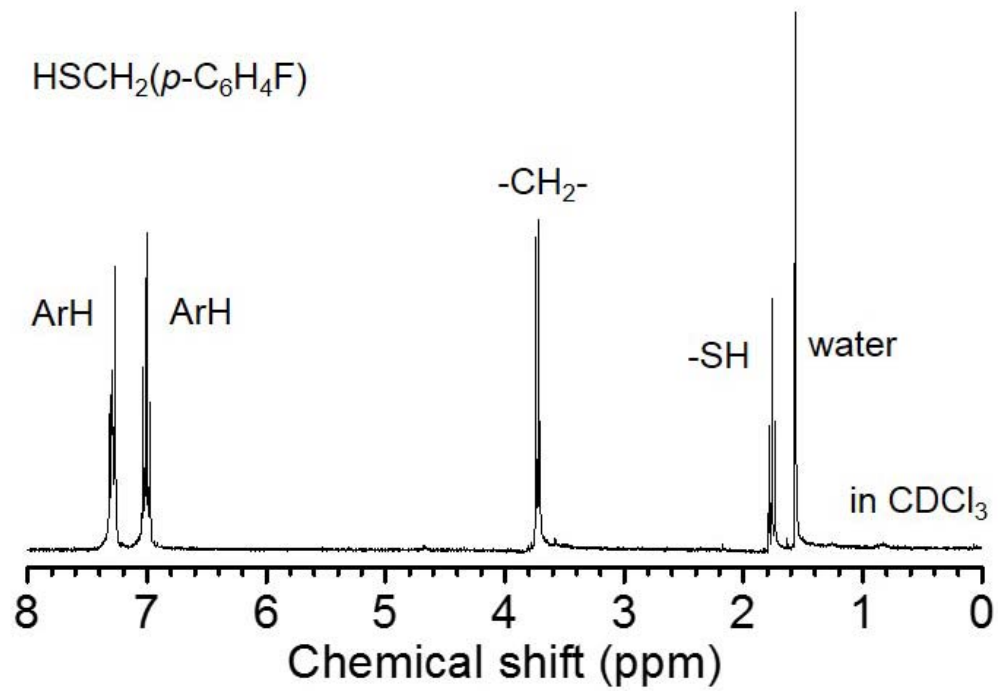
**Figure S13.** $^1H$ NMR spectrum for *p*-chlorobenzyl mercaptan in $CDCl_3$



$HSCH_2(p\text{-}C_6H_4Cl)$

ArH

-CH$_2$-

water

-SH

in CDCl$_3$

Chemical shift (ppm)
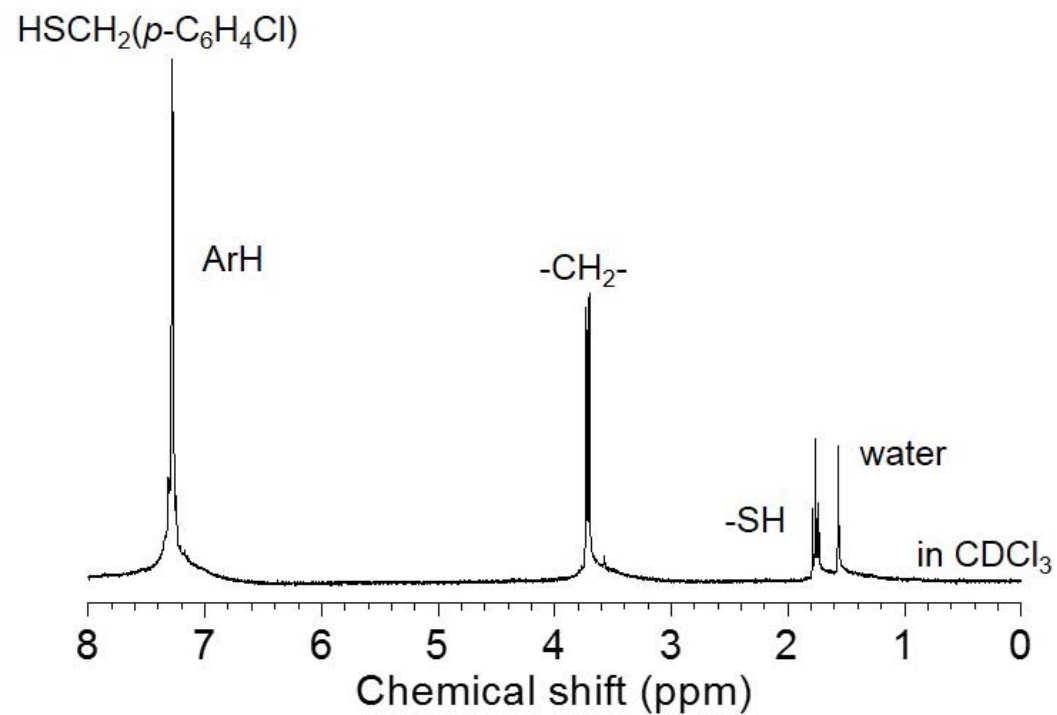
**Figure S14.** $^1H$ NMR spectrum for *p*-bromobenzyl mercaptan in $CDCl_3$



$HSCH_2(p\text{-}C_6H_4Br)$
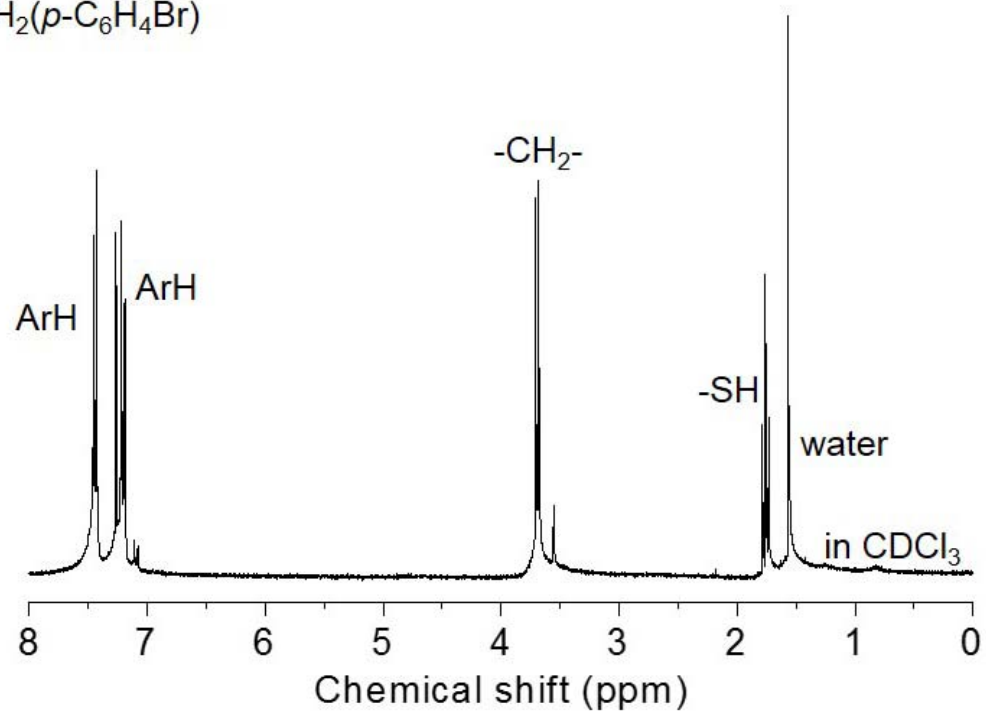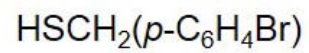
**Figure S15.** $^1$H NMR spectrum for *p*-iodobenzyl mercaptan in CDCl$_3$



HSCH$_2$(*p*-C$_6$H$_4$I)

-CH$_2$-

ArH    ArH

-SH

water
in CDCl$_3$

8    7    6    5    4    3    2    1    0
Chemical shift (ppm)
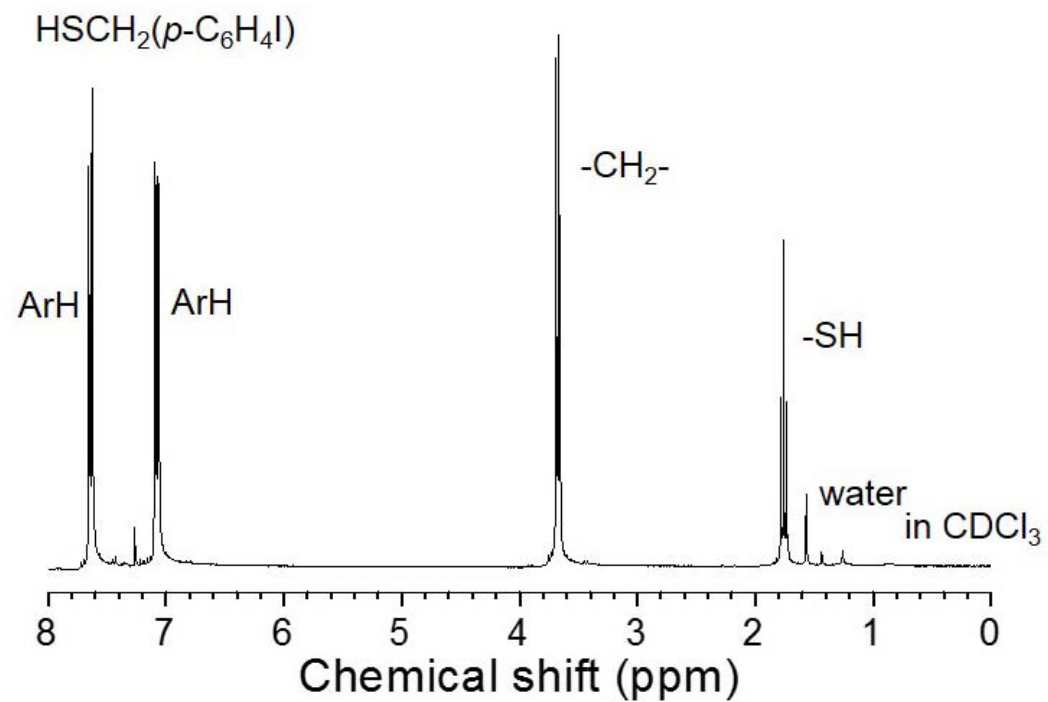
**Figure S16.** Representative photographs for contact angle measurements using a drop of deionized water (10µL) on the surface of SAMs of $Ag^{TS}/S(p-C_6H_4X)$.

a) X=H
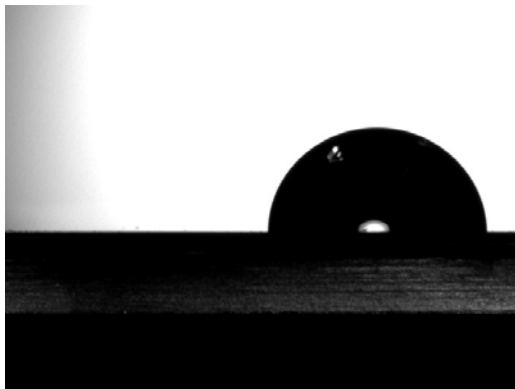


b) X=F
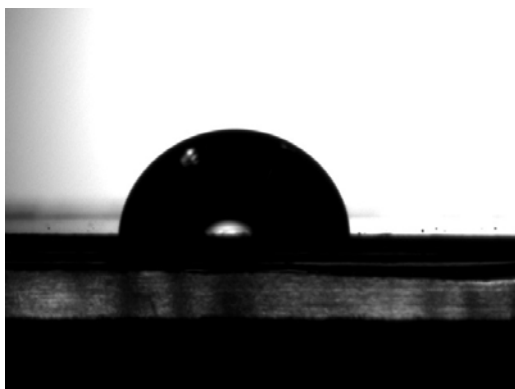


c) X=Cl
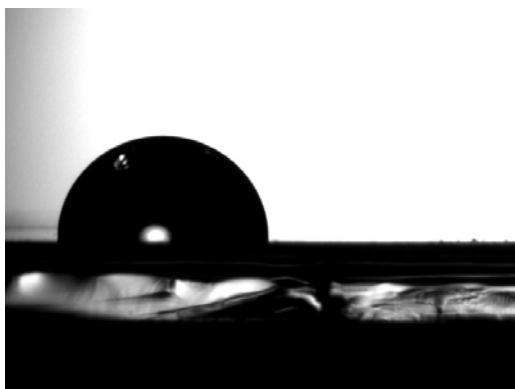
d) X=Br



e) X=I

**References**

1. S. Butini, S. Gemma, M. Brindisi, G. Borrelli, A. Lossani, A. M. Ponte, A. Torti, G. Maga, L. Marinelli, V. L. Pietra, I. Fiorini, S. Lamponi, G. Campiani, D. M. Zisterer, S.-M. Nathwani, S. Sartini, C. L. Motta, F. D. Settimo, E. Novellino and F. Focher, *J. Med. Chem.*, 2011, **54**, 1401–1420.
2. C. Amatore, S. Gazard, E. Maisonhaute, C. Pebay, B. Schöllhorn, J.-L. Syssa-Magalé and J. Wadhawan, *Eur. J. Inorg. Chem.*, 2007, 4035–4042.
3. H. J. Yoon, N. D. Shapiro, K. M. Park, M. M. Thuo, S. Soh and G. M. Whitesides, *Angew. Chem., Int. Ed.*, 2012, **51**, 4658-4661.
4. H. J. Yoon, C. M. Bowers, M. Baghbanzadeh and G. M. Whitesides, *J. Am. Chem. Soc.*, 2014, **136**, 16-19.
5. K.-C. Liao, H. J. Yoon, C. M. Bowers, F. C. Simeone and G. M. Whitesides, *Angew. Chem. Int. Ed.*, 2014, **53**, 3889-3893.
6. F. C. Simeone, H. J. Yoon, M. M. Thuo, J. R. Barber, B. Smith and G. M. Whitesides, *J. Am. Chem. Soc.*, 2013, **135**, 18131-18144.
7. C. M. Bowers, K.-C. Liao, H. J. Yoon, D. Rappoport, M. Baghbanzadeh, F. C. Simeone and G. M. Whitesides, *Nano Lett.*, 2014, **14**, 3521–3526.
8. M. M. Thuo, W. F. Reus, F. C. Simeone, C. Kim, M. D. Schulz, H. J. Yoon and G. M. Whitesides, *J. Am. Chem. Soc.*, 2012, **134**, 10876-10884.
9. D. G. Castner, K. Hinds and D. W. Grainger, *Langmuir*, 1996, **12**, 5083-5086.
10. B.-T. Teng, W.-X. Huang, F.-M. Wu, X.-D. Wen and S.-Y. Jiang, *Chem. Phys. Lett.*, 2008, **461**, 47-52.
11. H. J. Wu, H. K. Hsu and C. M. Chiang, *J. Am. Chem. Soc.*, 1999, **121**, 4433-4442.
12. H. F. Wang, X. Y. Deng, J. Wang, X. F. Gao, G. M. Xing, Z. J. Shi, Z. N. Gu, Y. F. Liu and Y. L. Zhao, *Acta Physico-Chimica Sinica*, 2004, **20**, 673-675.
13. M. M. Walczak, C. Chung, S. M. Stole, C. A. Widrig and M. D. Porter, *J. Am. Chem. Soc.*, 1991, **113**, 2370-2378.
14. M. Tencer, H.-Y. Nie and P. Berinia, *J. Electrochem. Soc.*, 2009, **156**, J386-J392.
15. M. Dimitriu, E. Filip and I. Humelnicu, *Rev. Chim. Bucuresti*, 2008, **59**, 1009-1013.